International Journal of Chemical, Materials and Biomolecular Sciences
ISSN: 2415-6620
Vol:5, No:11, 2011

Contact Drying Simulation of Particulate Materials: A Comprehensive Approach

Marco Intelvi, Apolinar Picado and Joaquín Martínez

***Abstract*—**In this work, simulation algorithms for contact drying of agitated particulate materials under vacuum and at atmospheric pressure were developed. The implementation of algorithms gives a predictive estimation of drying rate curves and bulk bed temperature during contact drying. The calculations are based on the penetration model to describe the drying process, where all process parameters such as heat and mass transfer coefficients, effective bed properties, gas and liquid phase properties are estimated with proper correlations. Simulation results were compared with experimental data from the literature. In both cases, simulation results were in good agreement with experimental data. Few deviations were identified and the limitations of the predictive capabilities of the models are discussed. The programs give a good insight of the drying behaviour of the analysed powders.

***Keywords*—**Agitated bed, Atmospheric pressure, Penetration model, Vacuum

I. Introduction

CONTACT dryers have been used successfully to dry a wide variety of products ranging from food and dairy products such as baby food, potato flakes, buttermilk powder, and coffee grounds sludge to chemical and other miscellaneous products such as carbon black, colloidal clay, pigments, peat, and many kinds of sludge. In general, contact dryers are drying equipments in which the heating medium, e.g. steam, hot gas, thermal fluids, does not come into contact with the product being dried. Instead, wet material is dried by contact with a heated surface; thus, heat transfer to the wet material is mainly by conduction from this surface. Contact dryer can, in principle, be operated both in presence of inert gas at atmospheric pressure (atmospheric contact drying) or in pure vapour atmosphere at reduced pressure (vacuum contact drying). A thorough comparison between convective and contact dryers in terms of advantages and disadvantages can be found in Kemp [1] and Menshutina and Kudra [2].

Contact drying may be regarded as an operation controlled by the efficiency of heat transfer from the wall to the particulate material [3,4]. Different modelling techniques for contact drying simulation have been proposed in the literature. The task of models is to reliably describe the supply of heat by contact of the assemblage of particles with the hot wall. This task can be accomplished either by continuous or by discrete models. Continuous models that assign effective properties to the bed of particles, especially the penetration model, are the present industrial standard. Intelvi [5] has summarised the penetration model developed by Schlünder and co-workers in the years 1975 to 1990. Schlünder and Mollekopf [3] have firstly investigated the vacuum contact drying of powder agitated bed in detail for a non-hygroscopic free flowing granular material and next extended by others authors to more complex cases including poly-dispersed materials [6], hygroscopic materials [7,8], materials with a binary mixture [9], modelling with particle intrinsic water transfer resistance [10], modelling with sticking particles and crust formation at heated wall [11]. As concerns atmospheric contact drying of powder agitated packed bed, some experimental data and theoretical analysis have been published by Tsotsas and Schlünder [12], Gevaudan and Andrieu [13] and more recently by Arlabosse and Chitu [14]. Although, the theoretical basis of contact drying, both vacuum and atmospheric, is established and available in the literature, there is a need for stable and reliable models to quantify and predict drying rates and drying times with a satisfactory accuracy for designing and optimising drying processes. The purpose of this study is the implementation of computer algorithms to simulate the contact drying process of particulate materials at atmospheric and vacuum conditions under a range of operating conditions and to demonstrate its use in an integrated methodology for process identification at the lab scale and prediction of drying times at the pilot or manufacturing scale. The validity of the models is tested by comparison of model predictions with experimental data from the literature.

II. Model Formulation

Two simulation algorithms one for vacuum and one for atmospheric contact drying of particulate materials are developed. In both cases, besides a mathematical model based on differential heat and mass balances in the wet bed of specified geometry, several models are used to estimate physical and thermodynamic properties [15], effective bed properties and heat and mass transfer coefficients. A qualitative scheme of the developed structure is shown in Fig. 1.

The partial financial support by the European Commission LLP/ERASMUS Programme is gratefully acknowledged.

M. Intelvi was with the Department of Chemical Engineering Principles and Practice, University of Padua, 35131 Padova, Italy (e-mail: marco.intelvi@hotmail.it).

A. Picado was with the National University of Engineering (UNI), PO Box 5595, Managua, Nicaragua. He is now with the Department of Chemical Engineering and Technology, Royal Institute of Technology (KTH), SE-100 44 Stockholm, Sweden (e-mail: picado@kth.se).

J. Martínez is with the Department of Chemical Engineering and Technology, Royal Institute of Technology (KTH), SE-100 44 Stockholm, Sweden (e-mail: martinez@kth.se).

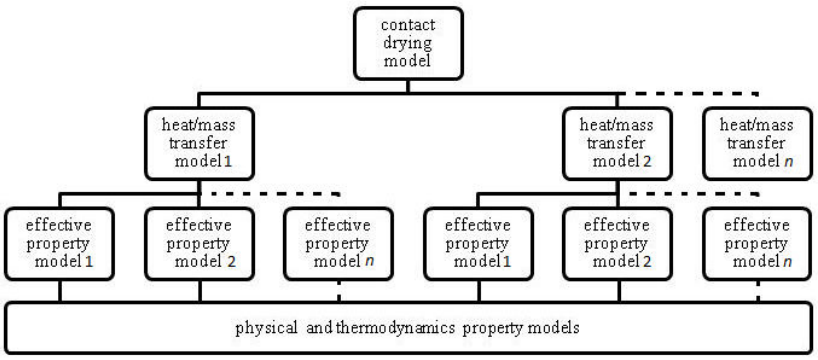

Fig. 1 Qualitative graphical representation of general *hierarchical structure* of the developed contact drying simulation models

A. Vacuum Contact Drying

A model for vacuum contact drying of agitated particulate materials based on the penetration theory is used [6]. The main model assumptions are:

- The bed is assumed as a quasi-continuum with effective properties.
- Temperature at the heating surface is assumed to be known.
- Distinct heating front parallel to the heating surface is move through the bed.
- Between the heating surface and the drying front the particles are dry, and beyond that the particles are still wet. In the wet part of the bed, the temperature is uniform and equal to the saturation temperature (T_s) of the liquid at the operating pressure. In the dry part of the bed, a temperature profile exists between the heating wall at T_w and the drying front at T_s (see Fig. 2).
- After a time period call *contact time*, instantaneous perfect macro-mixing is assumed inside the bed (mixing period), then the drying front penetration start again (contact period).

Also, the following transport phenomena are included:

- Contact heat transfer (from the heating wall to first particle layer).
- Penetration heat transfer (across the bed).

Internal mass and heat transport is neglected in the general case; thus, they are not modelled. Vapour mass transfer across the particle bed is also neglected. Other mass transport phenomena are not taken into account because of the vacuum.

In the first instant, the whole bed is at saturation condition therefore no heat penetration resistance occur. The only resistance is the heat contact resistance and the heat flux shows a maximum value. This value is the maximum drying rate for vacuum contact drying and it can be calculated by:

$$\dot{m}_{\max} = \frac{\dot{q}_0}{\Delta h_{ev}} = \frac{\alpha_{ws}\left(T_w - T_s(P)\right)}{\Delta h_{ev}} \tag{1}$$

where $\dot{q}_0$ is the heat flux at the heating wall and α_{ws} is the contact heat transfer coefficient and it is estimated as a sum of conduction in the contact point, conduction in the gas-filled gaps and radiative heat transfer [16].

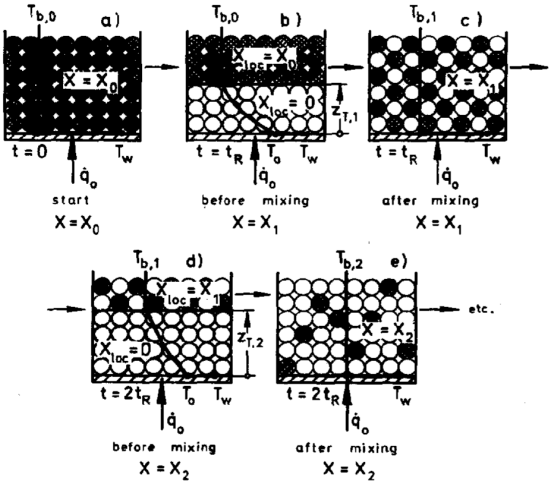

Fig. 2 Graphical representation of contact period and mixing period in penetration theory (after [3])

After this phase, the moisture content of the bed starts to fall down and the presence of dry particles in the bed produces a resistance in the heat penetration inside it. Thus,

$$\dot{m} = \frac{\dot{q}_{zT}}{\Delta h_{ev}} = \frac{\alpha_{ov}\left(T_w - T_b\right)\exp\left(-\varsigma^2\right)}{\Delta h_{ev}} \tag{2}$$

where $\dot{q}_{zT}$ is the heat flux at the drying front that is lower than the heat flux at the surface by the factor $\exp(\varsigma)$, because of the overheating of the already dry particles. ς is the reduced position of drying front and it can be evaluated using the penetration theory [3]. α_{ov} is the overall heat transfer coefficient during vacuum contract drying, gives by:

$$\frac{1}{\alpha_{ov,vac}} = \frac{1}{\alpha_{ws}} + \frac{1}{\alpha_{sb,vac}} \tag{3}$$

where $\alpha_{sb,vac}$ is the penetration heat transfer coefficient

across the dry bed, from the heating wall to the drying front, calculated by:

$$\alpha_{sb,vac} = \frac{2}{\sqrt{\pi}} \sqrt{\frac{\left(\lambda / \rho c_p\right)_{dry,bed}}{t_R}} \frac{1}{erf(\varsigma)} \tag{4}$$

The dry bed specific heat capacity $c_{p,bed}$ is assumed equal to the specific heat capacity of the particulate solid. The bulk density of the bed ρ_{bed} is calculated from the density of the non-porous solid by the following equation:

$$\rho_{dry,bed} = \rho_s (1-\varepsilon_b)(1-\varepsilon_p) \tag{5}$$

where ε is the porosity, the subscripts b and p denote bed and particle, respectively. The dry bed thermal conductivity λ_{bed} is estimated using the *parallel cell heat flux model* developed by Zehner [17] and Bauer [18]. In this approach, the thermal conductivity of dry bed is a function of the thermal conductivity of the solid, the thermal conductivity of the gaps between the particles and two equivalent thermal conductivities due to radiation and molecular flow. Finally, t_R is the contact time and it is estimated as:

$$t_R = t_{mix} N_{mix} \tag{6}$$

The first term can be assumed equal to the inverse of the stirring frequency, the second one, N_{mix}, is the mixing number and for it only empirical correlations are available in the literature. The correlation and the value of the coefficient proposed by Schlünder and Mollekopf [3] are used in the simulations.

An energy balance gives the temperature rise during each contact period. The equation used is:

$$\Delta T_b = \frac{\Delta h_{ev}}{c_{p,l}} \frac{1-\exp\left(-\varsigma^2\right)}{\exp\left(-\varsigma^2\right)} \Delta X \tag{7}$$

where T is the temperature and X is the solid moisture content in dry basis. The subscript l denotes liquid phase.

B. Atmospheric Pressure Contact Drying

The approach proposed by Tsotsas and Schlünder [12] is used to describe the atmospheric contact drying process (see Fig. 3). The main model assumptions are:

- The bed is assumed as a continuum with effective properties.
- Temperature at the heating surface is assumed to be known.
- The effect of particle mixing on drying rate is modelled following penetration theory. In this case, during contact period, there is no distinct drying front in the bed; whole bed is assumed partially wet.
- Unit value of Lewis number about the heat and mass transfer from the free surface of the bed to the bulk of the gas phase.
- No total pressure gradient exists within the bed; thus, no mass transfer resistance is assumed across the bed.

Also, the following transport phenomena are included:

- Contact heat transfer.
- Heat penetration transfer.
- Heat transfer to the gas phase above the bed.
- Mass transfer to the gas phase above the bed.

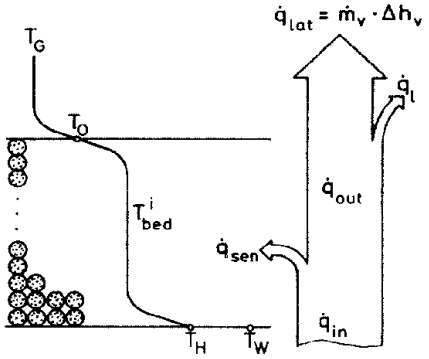

Fig. 3 Qualitative representation of temperature profiles and heat fluxes in contact drying at atmospheric pressure (after [12]).

Internal mass and heat transport is neglected in the general case and they are not modelled. Also mass transport phenomena across the particle bed are not taken in account. Evaluation of drying rate and the surface temperature T_0 can be done by simultaneous iterative solution of the following equations:

$$\left[\alpha_{sb,atm}(T_b - T_0)\right] - \left[(\alpha_c + \alpha_r)(T_0 - T_g)\right] = \dot{m}\Delta h_{ev}$$
$$\dot{m}\dot{Y} = \frac{MW_{liq}}{MW_{gas}} \frac{\alpha_c}{c_p} \left(\frac{P - p_g}{P - p_s(T_0)}\right) \tag{8}$$

The first equation is an energy balance, where $\alpha_{sb,atm}$ is the heat penetration transfer coefficient at atmospheric condition given by:

$$\alpha_{sb,atm} = \frac{2}{\sqrt{\pi}} \sqrt{\frac{\left(\lambda / \rho c_p\right)_{wet,bed}}{t_R}} \tag{9}$$

The wet bed specific heat capacity $c_{p,wet}$ is calculated by taking into account both the solid $c_{p,s}$ and moisture $c_{p,l}$ specific heat capacities:

$$c_{p,wet} = c_{p,s} + X c_{p,l} \tag{10}$$

The bulk density of the wet bed is calculated from the density of the non-porous solid and the density of the liquid by

the following equation:

$$\rho_{wet,bed} = v_s \rho_s (1-\varepsilon_b)(1-\varepsilon_p) + v_l \rho_l \quad (11)$$

where v is the volume fraction. The wet bed thermal conductivity $\lambda_{wet,bed}$ is estimated according to Zehner and Bauer model that is used also in vacuum contact drying modelling. In order to take into account the presence of the liquid phase, the model developed by Krischer is used [19].

In (8), α_c is the convective heat transfer coefficient in the gas phase estimated by empirical correlations from the literature; α_r is the radiative heat transfer coefficient. The second one equation is the interphase moisture mass transfer equation from the bed surface to the inert gas phase with a logarithmic drying force and unit Lewis number. If the saturation pressure is expressed as a function of T_0 by Antoine equation, the system has only 2 unknown variables $\dot{m}$ and T_0 and the solution can be reached. The values of $\dot{Q}_{out}$, $\dot{Q}_l$ and $\dot{Q}_{lat}$ can be calculated from other thermal balances [12].

III. Algorithm Implementation

The algorithms are based on a main iteration cycle, starting with initial moisture content and temperature of the bed. At each cycle, instantaneous moisture content, bed temperature variation and instantaneous drying rate are computed. The moisture content and temperature variation are used to calculate the new bed temperature for the next cycle. Every cycle represent a time step and its length is the maximum one for a stable and accurate solution. At every cycle, the value of all the physical properties of gas and liquid phases are updated at the new temperature; and also the effective properties are updated at the new value of physical properties, temperature and moisture content. The calculation cycle continues until the bed is totally dry ($X \leq 0$) or the time reach the "end time" of the simulation fixed as an input datum.

All calculations are made in several programs. There is a main program where the mass and energy balances in the dryer are solved and therefore drying rate and bed temperatures are calculated. The required heat and mass transfer coefficients and the effective properties are estimated in several sub-programs. At the end, a set of programs for physical and thermodynamic properties evaluation gives the value of the required properties. A graphical representation of the iteration cycle and the connection between the programs is shown in Fig. 4.

More detail about the algorithm structure for the vacuum and atmospheric cases can be found elsewhere [5].

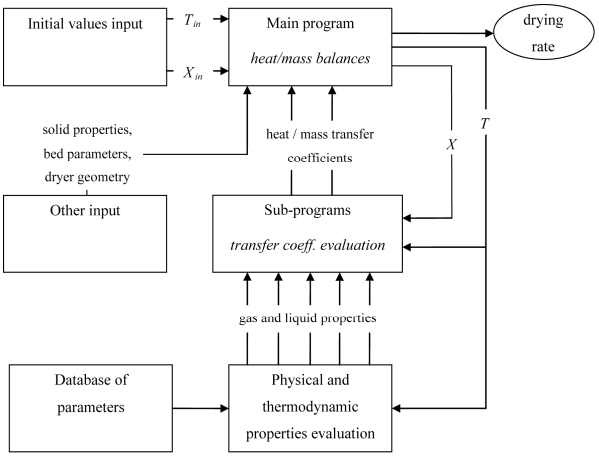

Fig. 4 Graphical representation of the iteration structure in contact drying programs

IV. Results and Discussion

A. Vacuum Contact Drying: Comparison with Experimental Data

A comparison between the simulation results and experimental data from the literature was conducted. The material under consideration is talc (indicated as MgSi). Details of the experimental procedure can be found elsewhere [3]. Drying rate curves of contact drying of the two talc powders wetted with water under vacuum in three kind of contact dryers are reported in the identified work. In this case, drying rate curves in the stirred disc dryer of 240 mm diameter were chosen and the program for vacuum contact drying of agitated beds was used to simulate the experimental data.

Most of the input data for the simulations are reported in [3], other data, in particular about the solid phase properties are taken from [20] and [21]. Further details on input data can be found in [5].

The results are depicted in Figs. 5 to 7 where experimental data of drying rate curves (dots) are compared with simulated drying rate curves (lines). The main input data for the simulation are reported in Table I.

Fig. 5 illustrates drying rate curves at three different heating wall temperatures. A good agreement between simulation results and experimental data is observed.

An enhancement of the drying rate is observed with the wall temperature increase. The rising in the wall temperature produce a increase in the temperature gradient between heating wall and particle bed that is the driving force to the heat transfer to the bed. Thus, with the rise up of the heat flux, a largest value of drying rate is obtained.

TABLE I
MAIN INPUT DATA FOR VACUUM CONTACT DRYING SIMULATION

		Units	Fig. 5	Fig. 6	Fig. 7
Initial values	Moisture content	kg/kg	0.25	0.18	0.25
Operating parameters	Pressure	kPa	1.60	4.5 / 7 / 17.5	0.19
	Wall temperature	°C	50.5 / 70.6 / 85.8	80	70.9
	Stirring frequency	rpm	15.4	30	0.2 / 1 / 45
Particle geometry	Diameter	mm	6	1.1	6
	Roughness	µm	20	2.5	20
Time length of one calculation step		s	0.2	0.05	0.01

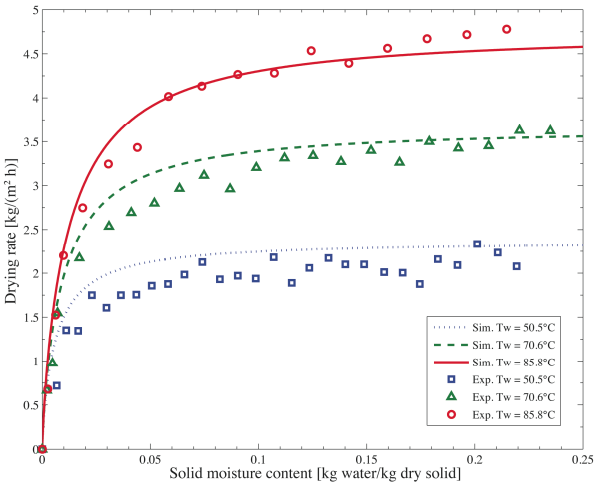

Fig. 5 Drying rate curves during vacuum contact drying of MgSi wetted with water at different heating wall temperatures

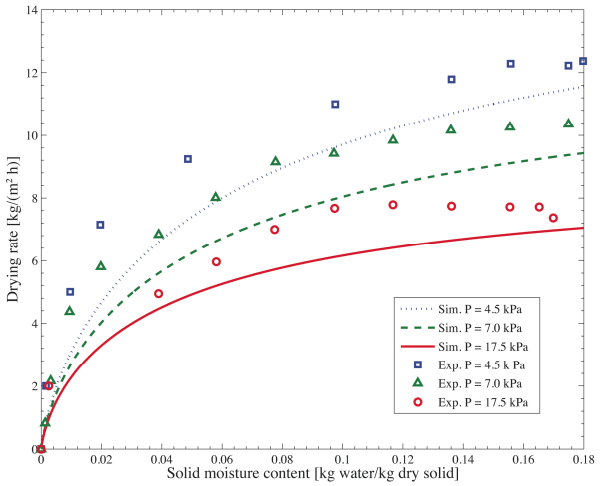

Fig. 6 Drying rate curves during vacuum contact drying of MgSi wetted with water at different pressures

Fig. 6 depicts drying rate curves at three different pressures. In this case, the mixing number estimated by the correlation proposed by Schlünder and Mollekopf [3] is 16.4 when the best fitting mixing number on this experimental dataset was found at 7.5. Graphical comparison between experimental data and simulated curve with the best fitting mixing number is reported elsewhere [5]. Pressure variation causes evident variation in the drying behaviour. The pressure effect is not direct, but is the variation of saturation temperature due to the pressure change that cause the different drying behaviour. In particular, when the pressure is fall down, the saturation temperature is fall down as well; then the bed temperature falls and the temperature gradient between heating wall and bed rise. This phenomenon produce an increase of the drying rate with the pressure falls.

Fig. 7 shows drying rate curves at three different stirring frequencies. Two simulations at 0.2 and 1 rpm show good agreement with the experimental data. The simulation at 45 rpm shows a small over-estimation of the drying rate.

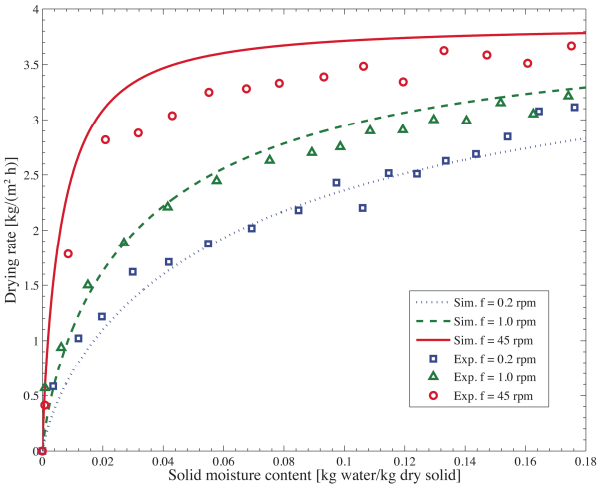

Fig. 7 Drying rate curves during vacuum contact drying of MgSi wetted with water at different stirring frequencies

In this case, no better results are obtained by changing the mixing number. Probably, there is a limit in the penetration theory to describe the effect of the particle motion on the drying rate at high stirring frequency. The stirring frequency variation caused a variation in the contact time, and then in the value of the heat penetration coefficient. In particular, if the stirring frequency rises up, the bed mixing is improved and the contact time become shorter and then the heat penetration coefficient rise up. Consequently, an increase in the drying rate is observed.

B. Atmospheric Contact Drying: Comparison with Experimental Data

A comparison between the simulation results and experimental data from the literature was conducted. The material under consideration is kaolin (indicated as AlSi). Details of the experimental procedure can be found elsewhere [12]. Experimental drying rate curves of AlSi wetted with water and dried in presence of air at atmospheric pressure are studied. The reported experimental data were obtained from a disc dryer of 100 mm diameter with a rotary stirring device, filled with a particle bed until 50 mm level. Also in this case, most of the input data for the simulations are reported in [12], other, in particular about the gas phase conditions are taken from other similar experiments of the same authors, see [5]. A summary of simulation input data is shown in Table II.

TABLE II
MAIN INPUT DATA FOR ATMOSPHERIC CONTACT DRYING SIMULATION

		Units	Fig. 8
Initial values	Moisture content	kg/kg	0.18
	Bed temperature	°C	20
	Pressure	kPa	101.325
	Wall temperature	°C	50 / 70 / 90
Operating parameters	Stirring frequency	rpm	63
	Solid hold up	kg	1.5
	Gas velocity	m/s	0.3
	Gas temperature	°C	40
	Gas abs. humidity	kg/kg	0.024
Particle geometry	Diameter	mm	4.353
	Roughness	μm	2.5
	Particle porosity	-	0.375
Computational parameters	Number of steps	-	558
	Step time length	s	5

The results are reported in Fig. 8, where experimental data, indicated by dots, are compared with the simulation results, indicated by lines.

The results show, in general, good agreement between experimental and simulated data. A deviation appeared for each one-simulation curve at the end of the process, for relative moisture content less than 0.1. In particular, as the moisture content goes to zero, the drying rate should go to zero as well, but in the simulated profiles did not happened. This behaviour was also noted by [12]. Probably, this deviation of the drying behaviour is due to the assumption of the used contact drying model. At the last stage of the drying process, when the moisture content is low, the intra-particle heat and mass transfer resistances could become the controlling resistances, but these phenomena were not modelled.

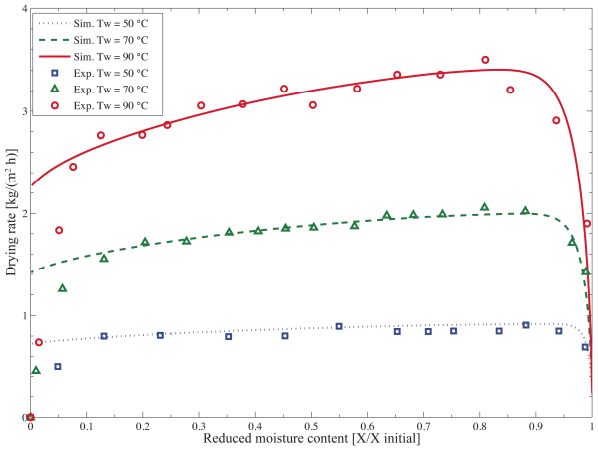

Fig. 8 Drying rate curves during the atmospheric contact drying of AlSi wetted with water in presence of air at different heating wall temperatures

An increase of drying rate is observed with a wall temperature rise-up. The reason of this behaviour is connected with the vaporisation mechanism. As the wall temperature rise up, the bed temperature rise up as well, then the saturation temperature of the moisture inside the bed increase. In this way, the partial pressure gradient between the moisture in the bed and the moisture in the gas phase increase and then the moisture vaporisation increase as well.

V. Conclusions

Two algorithms for agitated particle beds contact drying simulation, under two different operating conditions vacuum and atmospheric pressure, were developed. Penetration theory was used as the model to describe the drying process, mass and heat transfer coefficients and effective bed properties were estimated with different models from the literature, the liquid and gas phase properties were evaluated by proper correlations. Simulation results were compared with experimental data from the literature. For vacuum contact drying of agitated beds, in general, good agreement was found

with drying rate data of MgSi wetted with water and dried in an agitated disc dryer. The comparison of simulated drying rate curves with experimental drying rate data at atmospheric pressure show good agreement for most of the drying process. Only below the 0.1 % of moisture content, a deviation appeared. At this level of moisture content, internal resistance against mass transfer is probably not negligible. To extend the model to describe a process controlled by internal mass transfer, transport parameters of the solid are required. The main limitation on the application of the programs is the mixing number estimation. Only few empirical correlations are reported in the literature, referred to contact dryers. For industrial application, drying experiments should be done to find a proper empirical correlation or the empirical parameters for literature correlations. With further experimental validation, these programs could be a useful tool for design, analysis, optimisation and control of industrial contact dryers.

NOMENCLATURE

A	Heating wall area	m^2
c_p	Specific heat capacity	J kg^{-1} K^{-1}
Δh_{ev}	Latent heat of vaporisation	J kg^{-1}
Le	Lewis number	–
$\dot{m}_Y$	Drying rate	kg m^{-2} s^{-1}
$\dot{m}_{Y,\max}$	Drying rate, constant period	kg m^{-2} s^{-1}
m_s	Solid hold-up	kg
MW	Molar weight	kg kmol^{-1}
$\dot{n}_Y$	Molar drying rate	kmol m^{-2} s^{-1}
N_{mix}	Mixing number	–
p	Partial pressure	Pa
P	Pressure	Pa
$\dot{q}$	Heat flux	J m^{-2} s^{-1}
R	Universal gas constant	J kmol^{-1} K^{-1}
t	Time	s
t_R	Contact time	s
t_{mix}	Mixing time	s
T	Temperature	K
v	Volume fraction	–
X	Moisture content, dry basis	kg kg^{-1}

Greek symbols

α	Heat transfer coefficient	W m^{-2} K^{-1}
α_c	Convective heat transfer coefficient	W m^{-2} K^{-1}
α_{ov}	Overall heat transfer coefficient	W m^{-2} K^{-1}
α_r	Radiative het transfer coefficient	W m^{-2} K^{-1}
α_{sb}	Heat penetration coefficient	W m^{-2} K^{-1}
α_{ws}	Contact heat transfer coefficient	W m^{-2} K^{-1}
ε	Porosity	–
ς	Reduced instantaneous position of drying front	–
ρ	Density	kg m^{-3}
κ_{eff}	Effective thermal conductivity	m^2 s^{-1}

Subscripts

atm	Atmospheric case	*lat*	Latent
b	Bulk of the bed	*o*	At the free surface above the bed
bed	Referred to the particulate bed	*out*	Outside
dry bed	Dry bed property	*p*	Particle
eff	Effective property	*s*	Solid phase or saturation
g	of the gas phase	*vac*	Vacuum
gas	in the gas phase	*w*	At heating wall
in	Inside	*wet bed*	Wet bed property
l	Liquid phase	0	Initial

REFERENCES

[1] I. Kemp, "Progress in dryer selection techniques," *Drying Technol.*, vol. 17, pp. 1667-1680, 1999.
[2] N.V. Menshutina and T. Kudra, "Computer aided drying technologies," *Drying Technol.*, vol. 19, pp. 1825-1850, 2001.
[3] E.U. Schlünder and N. Mollekopf, "Vacuum contact drying of free flowing, mechanically agitated particulate material," *Chem. Eng. Process.*, vol. 18, pp. 93-111, 1984.
[4] K. Malhotra and M. Okazaki, "Contact drying in mechanically agitated granular beds: a review of fundamentals," in *Advances in Drying*, vol. 5, A.S. Mujumdar, Ed. Washington: Hemisphere Publishing Corporation, 1992, pp. 325.
[5] M. Intelvi, "Contact drying of particulate pharmaceuticals: modelling and simulation," MSc thesis, Dept. of Chemical Engineering Principles and Practice "I. Sorgato, University of Padova, Padova, Italy, 2010.
[6] E. Tsotsas and E.U. Schlünder, "Vacuum contact drying of free flowing mechanically agitated particulate multigranular packing," *Chem. Eng. Process.*, vol. 20, pp. 339-349, 1986.
[7] E. Tsotsas and E.U. Schlünder, "Vacuum contact drying of mechanically agitated beds: the influence of hygroscopic behaviour on the drying rate curve," *Chem. Eng. Process.*, vol. 21, pp. 199-208, 1987.
[8] R. Forbert and E. Heimann, "Vacuum contact drying of mechanically agitated: coarse, hygroscopic, bulk material," *Chem. Eng. Process.*, vol. 26, pp. 225-235, 1989.
[9] F. Heimann and E.U. Schlünder, "Vacuum contact drying of mechanically agitated granulate beds wetted with a binary mixture," *Chem. Eng. Process.*, vol. 24, pp. 75-91, 1988.
[10] D. Farges, M. Hemati, C. Laguérie, F. Vachet and P. Rousseaux, "A new approach to contact drying modeling," *Drying Technol.*, vol. 13, pp. 1317-1329, 1995.
[11] A. Dittler, T. Bamberger, D. Gehrmann and E.U. Schlünder, "Measurement and simulation of the vacuum contact drying of pastes in a LIST-type kneader drier," *Chem. Eng. Process.*, vol. 36, pp. 301-308, 1997.
[12] E. Tsotsas and E.U. Schlünder, "Contact drying of mechanically agitated particulate material in the presence of inert gas," *Chem. Eng. Process.*, vol. 20, pp. 277-285, 1986.
[13] A. Gevaudan and J. Andrieu, "Contact drying modeling of agitated porous media beds," *Chem. Eng. Process.*, vol. 30, pp. 31-37, 1991.
[14] P. Arlabosse and T. Chitu, "Identification of the limiting mechanism in contact drying of agitated sewage sludge," *Drying Technol.*, vol. 25, pp. 557-567, 2007.
[15] R.C. Reid, J.M. Prausnitz and B. Poling, *The Properties of Gases and Liquids*, 4th ed. Washington, USA: McGraw-Hill Companies, 1987.
[16] E.U. Schlünder, "Wärmeübergang an bewegte Kugelschüttungen bei kurzfristigem Kontakt," *Chem. Ing. Tech.*, vol. 43, pp. 651-654, 1971.
[17] P. Zhener, "Experimentelle und theoretische Bestimmung der effektiven Wärmeleitfähigkeit durchströmter Kugelschüttungen bei mäßigen und hohen Temperaturen," Dr.-Ing. Thesis, Institut für Thermische Verfahrenstechnik, Universität Karlsruhe, Karlsruhe, 1972.
[18] R. Bauer, "Effektive radiale Wärmeleitfähigkeit gasdurchströmter Schüttungen mit Partikeln unterschiedlicher Form und Größenverteilung," Dr.-Ing. Thesis, Institut für Thermische Verfahrenstechnik, Universität Karlsruhe, Karlsruhe, 1976.

[19] O. Krischer and W. Kast, *Die wissenschaftlichen Grundlagen der Trocknungstechnik*. Berlin: Springer-Verlag GmbH, 1978.
[20] R.J. Gummow and I. Sigalas, "The thermal conductivity of talc as a function of pressure and temperature," *Int. J. Thermophysics*, vol. 9, pp. 1111-1120, 1988.
[21] A. Michot, D.S. Smith, S. Degot and C. Gault, "Thermal conductivity and specific heat of kaolinite: Evolution with thermal treatment," *J. Eur. Ceram. Soc.*, vol. 28, pp. 2639-2644, 2008.